



THE UNIVERSITY *of* EDINBURGH

Edinburgh Research Explorer

Formation of Fluorohydroxyapatite with Silver Diamine Fluoride

Citation for published version:

Mei, ML, Nudelman, F, Marzec, B, Walker, JM, Walls, A, Chu, CH & Lo, ECM 2017, 'Formation of Fluorohydroxyapatite with Silver Diamine Fluoride', *Journal of Dental Research*, pp. 002203451770973. <https://doi.org/10.1177/0022034517709738>

Digital Object Identifier (DOI):

[10.1177/0022034517709738](https://doi.org/10.1177/0022034517709738)

Link:

[Link to publication record in Edinburgh Research Explorer](#)

Document Version:

Peer reviewed version

Published In:

Journal of Dental Research

General rights

Copyright for the publications made accessible via the Edinburgh Research Explorer is retained by the author(s) and / or other copyright owners and it is a condition of accessing these publications that users recognise and abide by the legal requirements associated with these rights.

Take down policy

The University of Edinburgh has made every reasonable effort to ensure that Edinburgh Research Explorer content complies with UK legislation. If you believe that the public display of this file breaches copyright please contact openaccess@ed.ac.uk providing details, and we will remove access to the work immediately and investigate your claim.



Formation of fluorohydroxyapatite with silver diamine fluoride

May L. Mei¹, Fabio Nudelman², Bartosz Marzec², Jessica M. Walker², Edward C. M. Lo¹, Angus W. Walls^{3*}, C. H. Chu^{1*}

¹ Faculty of Dentistry, The University of Hong Kong, Hong Kong SAR, China

² EaStCHEM, School of Chemistry, The University of Edinburgh, Joseph Black Building, David Brewster Road, Edinburgh EH9 3FJ, United Kingdom

³ Edinburgh Dental Institute, The University of Edinburgh, Edinburgh, United Kingdom

Keywords: caries, remineralisation, silver diamine fluoride, hydroxyapatite, apatite.

Correspondence: Prof. C.H.Chu

Faculty of Dentistry
The University of Hong Kong
34 Hospital Road,
Hong Kong SAR, China.
Tel: +852 2859 0287
Fax: +852 2858 7874
E-mail: chchu@hku.hk

Correspondence: Prof. A.W.Walls

Edinburgh Dental Institute
Lauriston Building (4th Floor)
Lauriston Place
Edinburgh EH3 9HA
United Kingdom
Tel: +44(0)131 536 4975
Fax: +44(0)131 536 4971
E-mail: angus.walls@ed.ac.uk

Abstract

Silver diamine fluoride (SDF) is found to promote remineralisation and harden the carious lesion. Hydroxyapatite crystallisation is a crucial process in remineralisation, however, the role of SDF in crystal formation is unknown. We designed an *in vitro* experiment using calcium phosphate with different SDF concentrations (0.38 mg/ml, 1.52 mg/ml, 2.66 mg/ml and 3.80 mg/ml) to investigate the effect of this additive on the nucleation and growth of apatite crystals. Two control groups, namely calcium phosphate ($\text{CaCl}_2 \cdot 2\text{H}_2\text{O} + \text{K}_2\text{HPO}_4$ in buffer solution) and SDF ($\text{Ag}(\text{NH}_3)_2\text{F}$ in buffer solution) were also prepared. After incubation at 37°C for 24 hrs, the shape and organisation of the crystals were examined by bright field transmission electron microscopy (TEM) and electron diffraction. Unit cell parameters of the obtained crystals were determined with powder X-ray diffraction (P-XRD). The vibrational and rotational modes of phosphate groups were analysed using Raman microscopy. The TEM and selected-area electron diffraction confirmed that all solids precipitated within the SDF groups were crystalline and that there was a positive correlation between the increased percentage of crystal size and the concentration of SDF. The P-XRD patterns indicated fluorohydroxyapatite and silver chloride were formed in all the SDF groups. Compared with calcium phosphate control, a contraction of the unit cell in the *a*-direction but not the *c*-direction in SDF groups was revealed, which suggested that small, localised fluoride anions substituted the hydroxyl anions in hydroxyapatite crystals. This was further evidenced by the Raman spectra, which displayed up-field shift of the phosphate band in all of the SDF groups and confirmed that the chemical environment of the phosphate functionalities indeed changed. The results suggested that SDF reacted with calcium and phosphate ions and produced fluorohydroxyapatite. This preferential precipitation of fluorohydroxyapatite with reduced solubility could be one of the main factors for arrest of caries lesions treated with SDF.

Background

Silver diamine fluoride (SDF) is a topical fluoride solution that has been used for caries management. Unlike other fluoride products which prevent the formation of new caries, SDF is capable of efficiently halting the caries process (Gao et al. 2016). Recently, this caries-arresting property of SDF has drawn much attention from dental clinicians and researchers. SDF has shown its clinical success on arresting the coronal caries of the primary teeth of children (Chu et al. 2002), permanent teeth in teenagers (Chu et al. 2014) and root caries of the elderly (Tan et al. 2010). An *in vitro* study found that SDF increases the mineral density of the artificial carious lesion (Mei et al. 2013b); *ex vivo* studies investigated the collected, exfoliated primary teeth from the SDF clinical trials and found a hardened and highly mineralised zone was formed in the outermost 150 μm of an SDF-treated carious lesion (Chu and Lo 2008; Mei et al. 2014b). Silver has a well-known antibacterial effect and previous studies demonstrated that SDF inhibited cariogenic biofilm formation (Chu et al. 2012; Mei et al. 2013a; Mei et al. 2013c).

However, there are only a few publications that report the mode of action of SDF on mineralised tissue. Yamaga et al. (1972) suggested that the formation of calcium fluoride (CaF_2) and silver phosphate (Ag_3PO_4) could be responsible for the prevention of dental caries and the hardening of a carious lesion. However, Suzuki et al. (1974) demonstrated the formation of CaF_2 by mixing enamel powder with an SDF solution, but the amount of CaF_2 dropped significantly when the materials were immersed into artificial saliva. They also found that Ag_3PO_4 disappeared after being immersed in artificial saliva, and was replaced by silver chloride (AgCl) and silver thiocyanate (AgSCN). In addition, Lou et al. (2011) found a CaF_2 -like material and metallic silver were formed by mixing SDF with hydroxyapatite powder and gelatine (as a chemically-representative protein), but the CaF_2 -like material dissolved and disappeared after washing with water. Therefore, the mode of SDF action is still unclear.

The high concentration of calcium and phosphate in saliva is the major mineral source in the oral environment. The contribution of calcium, phosphate and hydroxyl ions present in saliva to apatite deposition is fundamental. However, to the best of our knowledge, there has been no study to investigate the role of SDF as an additive in synthetic apatite crystallisation experiments. It is therefore worthwhile to study mineral structures formed in the presence of SDF to gain

insights into these complex reactions (Beniash et al. 2005). Thus, this study aimed to observe the effect of SDF on hydroxyapatite crystallisation occurring *in vitro*, whereby the observed apatite deposition was described using a simplified chemical model. The null hypothesis was that SDF had no effect on crystal formation.

Materials and methods

Mineralisation reaction

The reaction was performed in a Tris-buffered saline (TBS), consisting of a 50 mM Trizma base and 150 mM sodium chloride (NaCl) in Milli-Q water set at pH 7.40. Apatite precipitation was achieved by incubating CaCl_2 (5.88 mM, Merck Ltd., Darmstadt, Germany) with K_2HPO_4 (4.12 mM, Merck Ltd., Darmstadt, Germany) in TBS at 37 °C for 24h as described (Habraken et al. 2013), in the presence or absence of different concentrations of SDF: 0.38 mg/ml (fluoride concentration: 45 ppm), 1.52 mg/ml (fluoride concentration: 180 ppm), 2.66 mg/ml (fluoride concentration: 314 ppm) and 3.80 mg/ml (fluoride concentration: 448 ppm). These 4 groups containing SDF were called SDF groups. The calcium phosphate control contained $\text{CaCl}_2 + \text{K}_2\text{HPO}_4$, but no SDF. The SDF control comprised 0.38 mg/ml SDF in the TBS without $\text{CaCl}_2 \cdot 2\text{H}_2\text{O} + \text{K}_2\text{HPO}_4$. The final pH values of each reaction were measured using a pH electrode. Samples were then analysed using transmission electron microscopy (TEM) with Energy-dispersive X-ray spectroscopy (EDS), powder X-ray diffraction (P-XRD) and Raman spectroscopy (see below). The experiment was done in triplicate.

Transmission and scanning electron microscopy analysis

For TEM and EDS analysis, formvar/carbon-coated 200-mesh Ni TEM grids (Agar Scientific, Dorset, UK) were plasma treated for 40 seconds using a Quorum sputter-coater prior to use. The grids were floated upside-down over a 2 ml reaction solution in a 24-well plate. At the end of the reaction, the grids were rinsed with Milli-Q water, blotted against filter paper, air dried and analysed by TEM. TEM Analysis was performed using a Technai F20 (FEI) equipped with a field-emission gun and an $8\text{k} \times 8\text{k}$ Tietz CCD camera (Beniash et al., 2005). Ten crystal units were selected randomly from the TEM images, and the width and length of the crystal unit was measured using the image analysis software “imageJ” (National Institutes of Health, Bethesda, MD, USA). The changes in proportions of the crystals for each group were calculated based on

the difference between the means of each group divided by that of the calcium phosphate control group. Selected-area electron diffraction (SAED) was performed in order to determine the crystallographic parameters of the investigated samples. EDS was used to characterise the chemical composition of the precipitates and quantify the fluoride/calcium (F/Ca) and fluoride/phosphorus (F/P) ratios by dividing the mean atomic percentage of fluoride by either that of the calcium or that of the phosphorus.

Powder X-ray diffraction

The reaction solution was centrifuged at 5,000 g and the pellet was collected and washed thoroughly by Milli-Q water and re-suspended into ethanol. A drop (*ca.* 10 μ L) of this suspension was deposited on a low background Si-substrate and the solvent was allowed to evaporate. The samples were then analysed using a Bruker D2 Phaser P-XRD diffractometer equipped with a CuK α lamp ($\lambda = 1.54056$ Å). Data collection parameters included: 2θ range = $20-60^\circ$, step size = 0.02° and scan speed = 0.5 second/step. Hexagonal unit cell parameters a and c were calculated according to Bragg's equation (1), from the (300)- and (002)- reflections observed in the recorded P-XRD patterns (Liu et al., 2013).

$$d = \frac{n\lambda}{2 \sin \theta} \quad (1) \text{ (where } d \text{ – distance between symmetry equivalent diffraction planes, } n \text{ – consecutive natural number, } \lambda \text{ – wavelength, } \theta \text{ – incident angle of the X-ray beam)}$$

Raman spectroscopy

Raman spectra of the samples were recorded using a Renishaw InVia Raman microscope system (3 accumulations, 900 - 1500 cm^{-1} range) equipped with a 785 nm laser. The laser spot size was approximately 3 μm , focused on the growth electrode, and the power was kept below 1 $\text{mW}/\mu\text{m}^2$. All spectra were recorded at ambient temperature (Chen et al., 2015).

Statistical analysis

The length and width of the crystal were assessed for a normal distribution using Shapiro-Wilk test for normality. One-way ANOVA with Bonferroni post hoc tests were used to detect differences between groups. Analyses were performed with the computer software SPSS Statistics, V19.0 (IBM Corporation, Armonk, USA). The level of statistical significance was set at 0.05.

Results

The TEM images revealed the morphology of experimental groups and corresponding SEAD and EDS results. Apatite crystals formed in the absence of SDF exhibited the characteristic plate-shape morphology (Kokubo et al. 2003), SAED showed the typical reflections corresponding to the (211)-, (002)- and (112)- planes of apatite. EDS confirmed the presence of Ca and P (Figures 1A-C). The addition of increasing concentrations of SDF to the reaction resulted in a change in the morphology of the crystals, shifting from plate-shaped crystals (no SDF) to round-ended prismatic morphology (Figures 1D-O). SAED showed the reflections corresponding to the (002)-, (211)- and (112)- planes, confirming that these crystals were made of apatite. Furthermore, the recorded EDS spectra contained a signal attributed to fluoride, in addition to Ca and P, confirming that fluoride was present in the investigated apatite samples. Interestingly, as the concentration of SDF increased, the crystals became longer and thicker. The width of the crystals (mean \pm SD) were 14 \pm 4nm①, 33 \pm 3nm②, 79 \pm 14nm③, 117 \pm 17nm④ and 126 \pm 6nm⑤ in calcium phosphate control (no SDF), 0.38mg/ml SDF, 1.52 mg/ml SDF, 2.66 mg/ml SDF and 3.80mg/ml SDF groups, respectively (①<②<③<④,⑤; $p<0.001$). The length of the crystals (mean \pm SD) were 137 \pm 25①, 273 \pm 72nm②, 497 \pm 55nm③, 547 \pm 94nm④ and 650 \pm 49nm⑤ in calcium phosphate control (no SDF), 0.38mg/ml SDF, 1.52 mg/ml SDF, 2.66 mg/ml SDF and 3.80mg/ml SDF groups, respectively (①<②<③,④<⑤; $p<0.001$). Their aspect ratios (width

divided by the length) also changed, going from 0.10 to 0.19. There was a positive correlation between the increased percentage of crystal size and the concentration of SDF (Figure 2). The increase in the width was much larger than that of the length, which is reflected in the change in the aspect ratio ($m = 2.20$) that can be found in Figure 2A than that found in Figure 2B ($m = 0.91$). As expected, no hydroxyapatite crystal was detected in the SDF control (no calcium phosphate) group.

There was a steady increase of both F/Ca and F/P ratios in the crystal when SDF concentration went up (Table 1). The reaction conditions were alkaline in all the SDF groups and the pH values increased when SDF concentrations increased. The pH value measured in the group containing calcium phosphate was 7.07, this drop of pH from the original 7.40 suggested a hydroxyl ion was incorporated into crystal and more hydrogen ions were released (Habraken et al. 2013). All of the results indicate the formation of fluorohydroxyapatite in all of the SDF groups, whereby the fluoride content increased with SDF concentration.

The typical P-XRD pattern of the experimental groups is shown in Figure 3A. The P-XRD analysis indicated that the solids precipitated in the calcium phosphate control group scattered X-rays similarly to hydroxyapatite. However, the reflections in SDF groups were sharper than that in the calcium phosphate control group, in particular in the hydroxyapatite (211)-, and (300)-reflections. It was found that the (300)- reflections in SDF groups were shifted slightly from $\sim 32.3^\circ$ (2θ) to $\sim 33.2^\circ$ (2θ) compared to the calcium phosphate control group (Figure 3B). The (002)-reflection was not significantly changed. This pattern of reflection is similar to the one of fluorohydroxyapatite previously reported (Chen et al., 2005). These shifts also reflect the contraction of the calculated unit cell parameters, as summarised in Table 1. Apart from apatite, the strong reflections at 27.88° , 32.28° and 46.28° in the SDF groups and the SDF control group (no calcium phosphate) were coincident with silver chloride (AgCl) (111)-, (200)- and (220)-reflections, which suggested that AgCl precipitated as a separate phase in the SDF-containing samples. Traces of silver oxide were also detected in the 0.38 mg/ml SDF group.

The Raman spectra showed that all experimental groups displayed a strong PO_4^{3-} band at $\sim 960\text{ cm}^{-1}$, except for the SDF control (no calcium phosphate) group (Figure 4). The PO_4^{3-} band associated with the P-O stretch shifted from 961 cm^{-1} in calcium phosphate control group (no SDF) to $\sim 965\text{ cm}^{-1}$ in SDF groups, indicating a change of the phosphate group environment and suggesting – taking into account the composition of the reaction mixture - a substitution of the hydroxyl groups with more electronegative fluoride anions.

Discussion

This was the first study which investigated the effect of SDF on remineralisation progress in the context of crystal formation. The null hypothesis was rejected according to the results of this research. SDF clearly altered the crystal structure of the precipitated minerals and its presence enabled the formation of fluorohydroxyapatite. This observation helps to build the understanding of the role of SDF in the remineralisation of caries.

In this study, we adopted a buffered calcium phosphate system to perform the reaction, this system has been shown to be able to start an initial deposition of amorphous calcium phosphate and favours subsequent transformation into small crystals of apatite and ultimate growth of ripening of those crystals (Termine and Posner 1970). However, this might be different from real situation. Another limitation of the chemical system is the lack of biological component, in which the role of silver could be underestimated. This chemical system is very different from complex *in vivo* situation and thus caution should be exercised in data interpretation.

Although the commercial SDF solution (Saforide) has a high concentration of silver (255,000 ppm) and fluoride (448,000 ppm), clinical treatment will consist of a one-time application of a minute volume of the solution ($0.22 \pm 0.07\text{ mg}$) to carious lesions (Chu et al. 2012). In the clinical setting, the SDF will be readily diluted by saliva in the oral cavity. The volume of saliva in the mouth is around 0.60 mL (Lagerlöf F and Dawes C, 1984). The concentration of SDF per application is approximately $0.22/0.60$, namely 0.36 mg/ml . Base on this assumption, we arbitrarily selected several concentrations from 0.38 mg/ml to 3.80 mg/ml in this study.

Saliva plays a crucial role in the caries remineralisation progress. It is a buffered system, supersaturated with respect to calcium phosphate, whereby proline- and tyrosine-rich proteins inhibit the excessive nucleation of apatite phases (Schwartz SS et al. 1992). The salivary activities of calcium and phosphate ions are important because both species are part of the hydroxyapatite unit cell. Therefore saliva offers a protective and reparative environment for teeth. The calcium and phosphate ions provided by $\text{CaCl}_2 + \text{K}_2\text{HPO}_4$ in TBS were a basic simulation of this salivary environment. TEM grids were explicitly floated upside-down during the incubation to prevent the sedimentation of particles formed by homogeneous nucleation on their surfaces (Majewski and Allidi 2006). In this study, we demonstrated that SDF reacted with calcium and phosphate from salivary environment and form fluorohydroxyapatite. Apart from salivary environment, the residual mineral crystals of the tooth could be another important factor of remineralisation, it serves as nucleation site for the newly formed fluorohydroxyapatite to precipitate (Peters et al. 2010), or promotes the ion exchange of F^- for OH^- (Ogard et al. 1994). However, the exchange of the F^- for OH^- requires an acidic micro-environment to dissolve the tooth mineral in order to release OH^- . SDF is very alkaline (pH around 10). This alkaline property matches the favourable condition to synthesis fluorohydroxyapatite in chemistry (Chen and Miao 2005) which may fasten the reaction process by promoting precipitation.

The hydrogen ions (H^+) of the hydroxyapatite were arranged in the atomic interstices neighbouring the oxygen ions (O^{2-}). The OH^- conferred a certain degree of disorder to the crystal structure of hydroxyapatite (Chen and Miao 2005). An increase in the vibrational frequency of phosphate group in SDF groups was observed in Raman spectra, which indicates the substitution of OH^- with more electronegative F^- (Chen et al. 2015). The isotropic distribution of charge on F^- anions allows for a better fit in the lattice compared to the larger asymmetric OH^- ion (Robinson et al. 2004), thus reducing lattice microstrain and enabling fluorohydroxyapatite crystals to form larger particles. This alternating arrangement produces a fairly well-ordered apatite structure, which is characterised with increased thermal and chemical stability when compared with hydroxyapatite (Chen and Miao 2005). In addition, since F^- is smaller than OH^- , the substitution also results in a noticeable contraction in the a -axis dimensions of the lattice (Table 1) (Liu et al. 2013; Wei et al. 2003).

The P-XRD pattern showed that calcium phosphate control group diffracted poorly (Figure 3). It is plausible that the unit cell of calcium phosphate was large and flexible enough to accommodate other matters. This reduced X-ray coherence length and resulted in broader reflections with low intensities. P-XRD relies on Bragg's Law. There is no scattering when there is no *d*-spacing. In addition, The Ca/P ratio was 1.95 in the 0.38 mg/ml SDF group. However, for the SDF concentrations at or higher than 1.52 mg/ml, the ratios varied between 1.48 and 1.62, which was consistent with apatite minerals. Furthermore, EDS provided a semi-quantitative view of the elemental composition in the inspection field in units of weight/atomic percent. It might not be suitable to determine the precise stoichiometric determination of the ratios between calcium and phosphate in the samples.

We detected enlarged apatite crystal sizes in the SDF groups and the size of the crystals increased with the increase in SDF concentration. This is consistent with a previous bone study which showed that fluoride uptake is accompanied by an increase in the apatite crystal size (Eanes and Hailer 1998). It is plausible that the introduction of well localised, isotropic, negatively charged F⁻ increases the stability of the structure and reduces the amount of defects related to the lattice strain. Therefore, single-crystalline domains may grow larger before their growth is interrupted by a crack or irreparable dislocation. We also found that this increase of crystal size took place predominantly in its width but not in its length (Figure 2). Fluoride stabilised preferentially the lateral growth against aberrant outgrowths, thus promoting a more orderly growth of new accretion layers (Eanes and Hailer 1998). The collagen matrix plays an important organisational role in establishing the manner of the crystal arrangements as well as placing some spatial constraints on their size and shape (Eanes and Hailer 1998). Further studies can be performed to address this aspect.

We did not find CaF₂, which was probably attributed to the low concentration of SDF used in this study. Other studies found that CaF₂ was not stable (Lou et al. 2011; Suzuki et al. 1974). The amount of CaF₂ significantly dropped after being immersed into artificial saliva (Suzuki et al. 1974) or disappeared after washing with water (Lou et al. 2011). Although immersing into artificial saliva or washing with water was to mimic the salivary fluid in clinical situation, this way of rinsing samples after exposure to SDF was susceptible to remove surface precipitation.

Ogard et al. (1994) showed that CaF_2 serve as a source of fluoride for the formation of fluorapatite. However, other investigators questioned the formation of CaF_2 within clinically relevant exposure times from concentrated fluoride solutions (Attin et al. 1995, Bruun and Givskov 1993). Attin et al. (1995) showed that 80% of the CaF_2 was lost in 5 days after fluoride varnish application. Bruun and Givskov (1993) reported that CaF_2 (or its likes) was not formed in measurable amounts on sound tooth. It is generally agree that a fluoride-releasing reservoir system is effective at low pH (Ogard et al. 1994; ten Cate 1997). SDF is alkaline. Its mechanism can be different from other acidic fluoride products. We found that SDF played a role in crystallisation and induced the formation of fluorohydroxyapatite. The signature of silver was not detected in the TEM/EDS experiment, which confirms that silver ions do not occlude within the newly formed fluorohydroxyapatite lattice. The only species originating from SDF that clearly had an effect on fluorohydroxyapatite precipitation were the fluoride anions that substituted the hydroxyl ions in the crystal.

Apart from calcium phosphate, silver chloride is a principal silver product that was detected using P-XRD. This result is consistent with previous studies (Mei et al. 2013b; Suzuki et al. 1974). Silver chloride has a low solubility of 8.9×10^{-5} g/100 ml, which might also contribute to the increased hardness of a carious lesion. Nevertheless, it has been shown that a silver ion has an antibacterial effect against cariogenic bacteria (Chu et al. 2012; Mei et al. 2013a; Mei et al. 2013c) and inhibits the collagenases degrading of dentine collagen (Mei et al. 2014a; Mei et al. 2012).

In summary, the present study demonstrated that SDF reacts with calcium and phosphate ions and produce fluorohydroxyapatite. This preferential precipitation of fluorohydroxyapatite with reduced solubility could be one of the main factors for arrest of caries lesions treated with SDF.

Author Contributions

ML Mei contributed to conception, design, data acquisition, analysis and interpretation and drafted the manuscript; F Nudelman contributed to conception and design and critically revised the manuscript; B Marzec and J Walker contributed to data interpretation and critically revised the manuscript; ECM Lo contributed to conception and critically revised the manuscript; AW Walls and CH Chu contributed to conception, design, data interpretation and critically revised the manuscript. All authors gave final approval and agree to be accountable for all aspects of the work.

Acknowledgment

This study was supported by Hong Kong - Scotland Partners in Post-Doctoral Research 2015/16 (S-HKU701/15), HKU Seed Fund for Basic Research (No. 201611159029), the Biotechnology and Biological Sciences Research Council (BBSRC, UK) Grant N^o. BB/M029611/1, the Wellcome Trust equipment grant WT087658 and the Scottish Life Science Alliance (SULSA).

Conflict of Interest Statement

The research presented in this paper is original. The authors declare no potential conflicts of interest with respect to the authorship and/or publication of this article.

References

- Attin T, Hartmann O, Hilgers RD, Hellwig E. 1995. Fluoride retention of incipient enamel lesions after treatment with a calcium fluoride varnish *in vivo*. Arch Oral Biol. 40(3):169-174.
- Beniash E, Simmer JP, Margolis HC. 2005. The effect of recombinant mouse amelogenins on the formation and organization of hydroxyapatite crystals *in vitro*. J Struct Biol. 149(2):182-190.
- Bruun C, Givskov H. 1993. Calcium fluoride formation in enamel from semi- or low-concentrated f agents *in vitro*. Caries Res. 27(2):96-99.
- Chen JS, Yu ZW, Zhu PZ, Wang JF, Gan ZH, Wei J, Zhao YH, Wei SC. 2015. Effects of fluorine on the structure of fluorohydroxyapatite: A study by XRD, solid-state NMR and Raman spectroscopy. J Mater Chem B. 3(1):34-38.
- Chen Y, Miao X. 2005. Thermal and chemical stability of fluorohydroxyapatite ceramics with different fluorine contents. Biomaterials. 26(11):1205-1210.
- Chu CH, Lee AH, Zheng L, Mei ML, Chan GC. 2014. Arresting rampant dental caries with silver diamine fluoride in a young teenager suffering from chronic oral graft versus host disease post-bone marrow transplantation: A case report. BMC Res Notes. 7:3.
- Chu CH, Lo EC. 2008. Microhardness of dentine in primary teeth after topical fluoride applications. J Dent. 36(6):387-391.
- Chu CH, Lo EC, Lin HC. 2002. Effectiveness of silver diamine fluoride and sodium fluoride varnish in arresting dentin caries in chinese pre-school children. J Dent Res. 81(11):767-770.
- Chu CH, Mei L, Seneviratne CJ, Lo EC. 2012. Effects of silver diamine fluoride on dentine carious lesions induced by streptococcus mutans and actinomyces naeslundii biofilms. Int J Paediatr Dent. 22(1):2-10.
- Eanes ED, Hailer AW. 1998. The effect of fluoride on the size and morphology of apatite crystals grown from physiologic solutions. Calcif Tissue Int. 63(3):250-257.
- Gao SS, Zhao IS, Niraishi N, Duangthip D, Mei ML, Lo EC, Chu CH. 2016. Clinical trials of silver diamine fluoride in arresting caries among children a systematic review. JDR Clinical & Translational Research. 1:201-210.
- Habraken WJEM, Tao JH, Brylka LJ, Friedrich H, Bertinetti L, Schenk AS, Verch A, Dmitrovic V, Bomans PHH, Frederik PM et al. 2013. Ion-association complexes unite classical and non-classical theories for the biomimetic nucleation of calcium phosphate. Nat Commun. 4.
- Kokubo T, Kim HM, Kawashita M. 2003. Novel bioactive materials with different mechanical properties. Biomaterials. 24(13):2161-2175.
- Lagerlöf F, Dawes C. 1984. The volume of saliva in the mouth before and after swallowing. J Dent Res. 63(5):618-21.

- 374 Liu Y, Hsu CY, Teo CM, Teoh SH. 2013. Potential mechanism for the laser-fluoride effect on
375 enamel demineralization. J Dent Res. 92(1):71-75.
- 376 Lou YL, Botelho MG, Darvell BW. 2011. Reaction of silver diamine [corrected] fluoride with
377 hydroxyapatite and protein. J Dent. 39(9):612-618.
- 378 Majewski PJ, Allidi G. 2006. Synthesis of hydroxyapatite on titanium coated with organic self-
379 assembled monolayers. Mat Sci Eng a-Struct. 420(1-2):13-20.
- 380 Mei ML, Chu CH, Low KH, Che CM, Lo EC. 2013a. Caries arresting effect of silver diamine
381 fluoride on dentine carious lesion with s. Mutans and l. Acidophilus dual-species cariogenic
382 biofilm. Med Oral Patol Oral Cir Bucal. 18(6):e824-831.
- 383 Mei ML, Ito L, Cao Y, Li QL, Chu CH, Lo EC. 2014a. The inhibitory effects of silver diamine
384 fluorides on cysteine cathepsins. J Dent. 42(3):329-335.
- 385 Mei ML, Ito L, Cao Y, Li QL, Lo EC, Chu CH. 2013b. Inhibitory effect of silver diamine
386 fluoride on dentine demineralisation and collagen degradation. J Dent. 41(9):809-817.
- 387 Mei ML, Ito L, Cao Y, Lo EC, Li QL, Chu CH. 2014b. An *ex vivo* study of arrested primary
388 teeth caries with silver diamine fluoride therapy. J Dent. 42(4):395-402.
- 389 Mei ML, Li QL, Chu CH, Lo EC, Samaranayake LP. 2013c. Antibacterial effects of silver
390 diamine fluoride on multi-species cariogenic biofilm on caries. Ann Clin Microbiol
391 Antimicrob. 12:4.
- 392 Mei ML, Li QL, Chu CH, Yiu CK, Lo EC. 2012. The inhibitory effects of silver diamine
393 fluoride at different concentrations on matrix metalloproteinases. Dent Mater. 28(8):903-908.
- 394 Ogard B, Seppa L, Rolla G. 1994. Professional topical fluoride applications--clinical efficacy
395 and mechanism of action. Adv Dent Res. 8(2):190-201.
- 396 Peters MC, Bresciani E, Barata TJ, Fagundes TC, Navarro RL, Navarro MF, Dickens SH. 2010.
397 In vivo dentin remineralization by calcium-phosphate cement. J Dent Res. 89(3):286-91.
- 398 Robinson C, Connell S, Kirkham J, Brookes SJ, Shore RC, Smith AM. 2004. The effect of
399 fluoride on the developing tooth. Caries Res. 38(3):268-276.
- 400 Schwartz SS, Hay DI, Schluckebier SK. 1992. Inhibition of calcium phosphate precipitation by
401 human salivary statherin: structure-activity relationships. Calcif Tissue Int. 50(6):511-7.
- 402 Suzuki T, Nishida M, Sobue S, Moriwaki Y. 1974. Effects of diammine silver fluoride on tooth
403 enamel. J Osaka Univ Dent Sch. 14:61-72.
- 404 Tan HP, Lo EC, Dyson JE, Luo Y, Corbet EF. 2010. A randomized trial on root caries
405 prevention in elders. J Dent Res. 89(10):1086-1090.

Termine JD, Posner AS. 1970. Calcium phosphate formation in vitro. I. Factors affecting initial phase separation. Arch Biochem Biophys. 140(2):307-317.

Wei M, Evans JH, Bostrom T, Grondahl L. 2003. Synthesis and characterization of hydroxyapatite, fluoride-substituted hydroxyapatite and fluorapatite. J Mater Sci Mater Med. 14(4):311-320.

Yamaga R, Nishino M, Yoshida S, Yokomizo I. 1972. Diammine silver fluoride and its clinical application. J Osaka Univ Dent Sch. 12:1-20.

Table 1. Calculated hexagonal unit cell parameters *a* and *c* axes, F/Ca, F/P and final pH, in experimental groups. All the data are normally distributed.

Group *	P-XRD		F/Ca	F/P	Final pH
	<i>a</i> -axis (Å)	<i>c</i> -axis (Å)			
No SDF (Calcium phosphate control)	9.577(±0.0012)	6.833(±0.0010)	N/A	N/A	7.07(±0.02)
0.38 mg/ml SDF	9.554(±0.0011)	6.833(±0.0010)	0.022(±0.002)	0.043(±0.006)	8.02(±0.01)
1.52 mg/ml SDF	9.552(±0.0036)	6.833(±0.0010)	0.037(±0.007)	0.055(±0.006)	8.14(±0.01)
2.66 mg/ml SDF	9.548(±0.0024)	6.833(±0.0010)	0.043(±0.004)	0.070(±0.009)	8.60(±0.02)
3.80 mg/ml SDF	9.542(±0.0047)	6.833(±0.0010)	0.072(±0.005)	0.111(±0.011)	8.95(±0.01)

* No crystal was detected in the SDF control (no calcium phosphate) group

Figure 1. TEM data of experimental groups

A: Morphology of calcium phosphate control group, B: SAED pattern of calcium phosphate control group;
C: EDS spectra of calcium phosphate control group;
D: Morphology of 0.38 mg/ml SDF group, E: SAED pattern of 0.38 mg/ml SDF group; F: EDS spectra of
0.38 mg/ml SDF group;
G: Morphology of 1.52 mg/ml SDF group, H: SAED pattern of 1.52 mg/ml SDF group; I: EDS spectra of
1.52 mg/ml SDF group;
J: Morphology of 2.66 mg/ml SDF group, K: SAED pattern of 2.66 mg/ml SDF group; L: EDS spectra of
2.66 mg/ml SDF group;
M: Morphology of 3.80 mg/ml SDF group, N: SAED pattern of 3.80 mg/ml SDF group; O: EDS spectra of
3.80 mg/ml SDF group.

* No crystal was detected in SDF control (no calcium phosphate) group

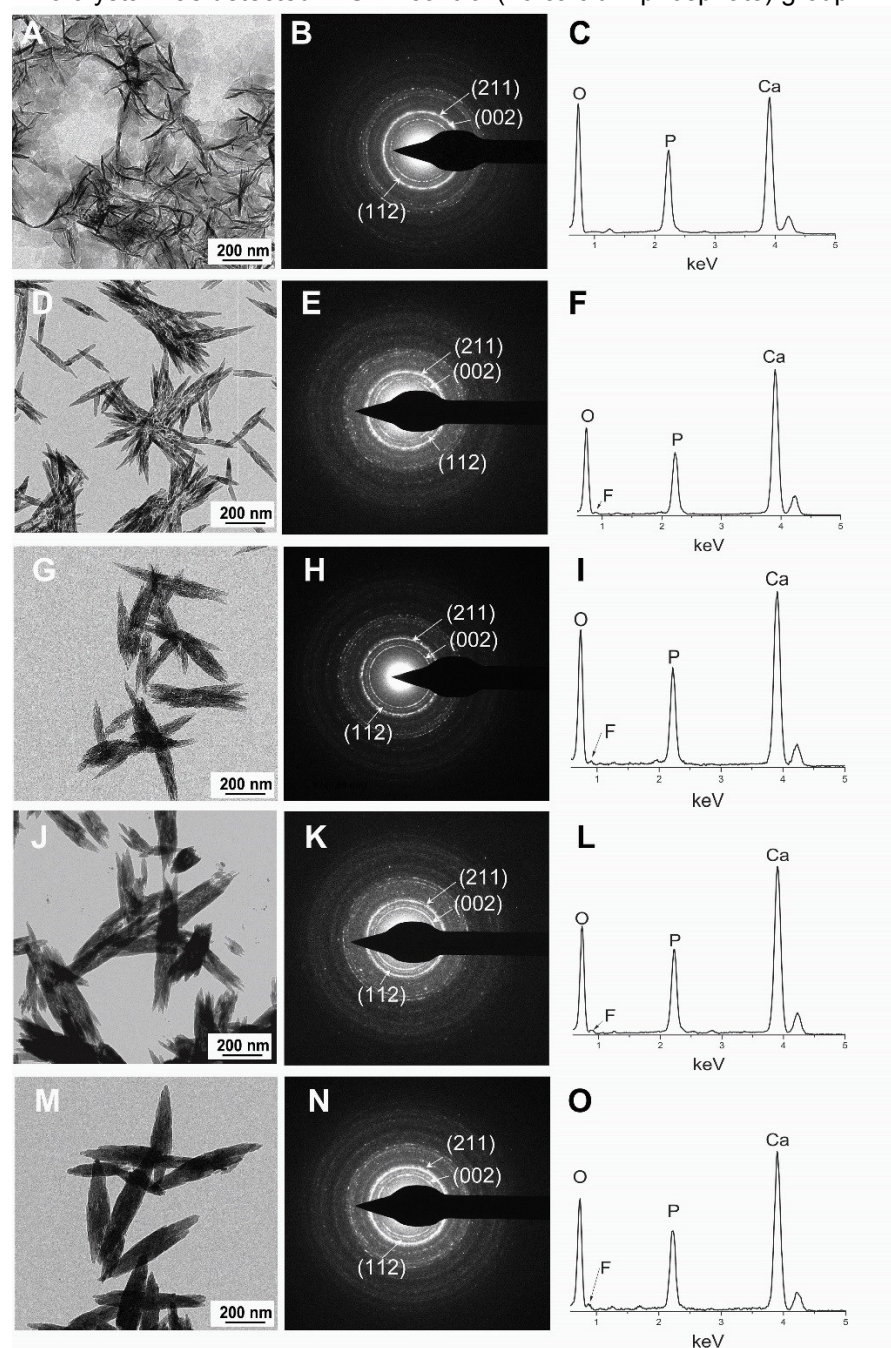


Figure 2. Pearson correlation between the percentage increase of crystal size and SDF concentrations

A: The correlation between percentage increase of width of crystal and SDF concentration (coefficient $R^2 = 0.95$, slope $m = 2.20$)
B: The correlation between percentage increase of length of crystal and SDF concentration (coefficient $R^2 = 0.90$, slope $m = 0.91$)

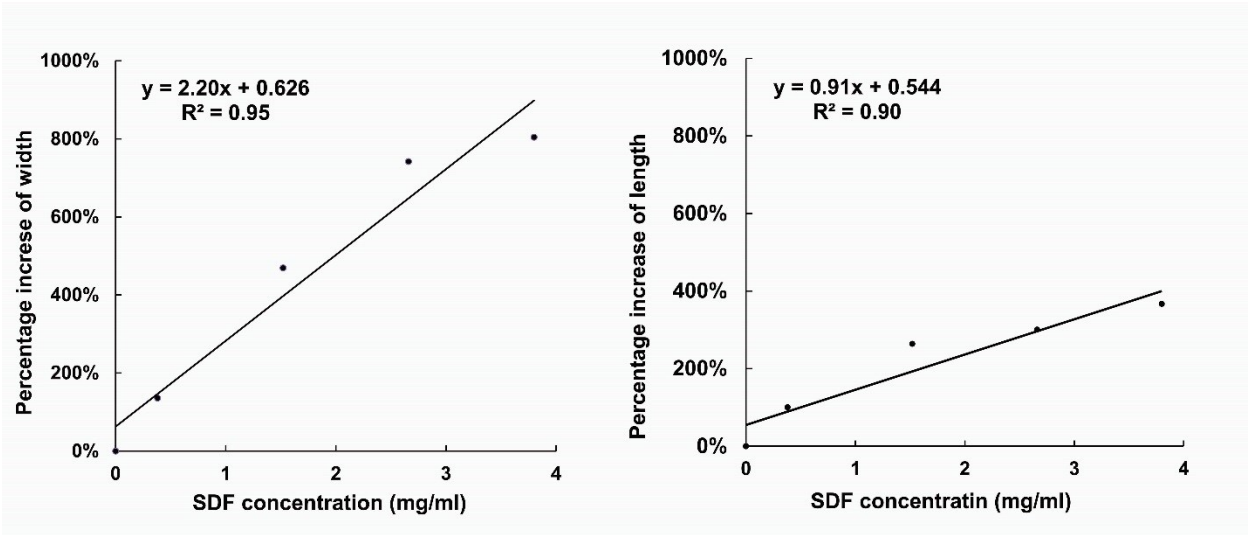


Figure 3. Typical P-XRD patterns of the experimental groups;

A: in range of 20 – 60°; B: in range of 30 – 35°

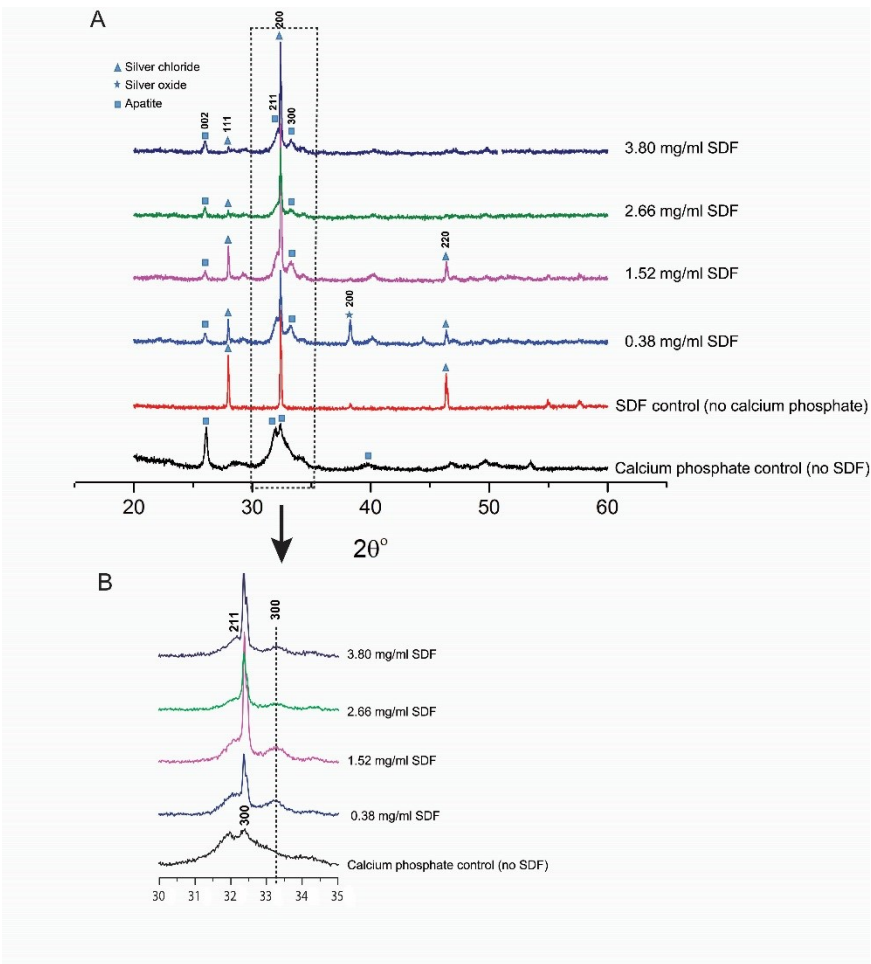


Figure 4. Raman vibrational spectra of the experimental groups in range of 930 – 1000 cm^{-1}

